Fabrication and characterization of green light emitting diode

Shirin SIAHJANI[1,2]**, Matthew WHITE**[1]**, Niyazi Serdar SARICIFTCI**[1]**,**
Sule ERTEN-ELA[2,*]

[1]Linz Institute for Organic Solar Cells, Institute of Physical Chemistry, Johannes Kepler University,
Linz, Austria
[2]Solar Energy Institute, Ege University, Bornova, İzmir, Turkey

Abstract: Phosphorescent polymer light emitting diodes (PLEDs) have been fabricated and characterized. A PLED was configured in an ITO/PEDOT:PSS/TPD:PBD:PVK:Ir(mppy)$_3$/LiF/Al device structure. Thicknesses of the active layer were optimized for an efficient phosphorescent organic light-emitting diode (OLED) device. The uniform mixing of the active layer was varied with different thicknesses. A hole transport layer of PEDOT:PSS was deposited in a thickness of 35 nm and an emissive layer of TPD:PBD:PVK:Ir(mppy)$_3$ was deposited in thicknesses of 90 nm, 56 nm, 40 nm, and 35 nm. The 56 nm thickness of the active layer was determined as the proper thickness according to results of current density, luminance, and voltage characteristics of the PLED. The processed PLED device exhibited a turn-on voltage of 3.6 V and a maximum luminance of 575.5 cd m^{-2} at 2.8 mA.

Key words: Organic active layer thickness, OLED, PVK, TPD, Ir(mppy)$_3$
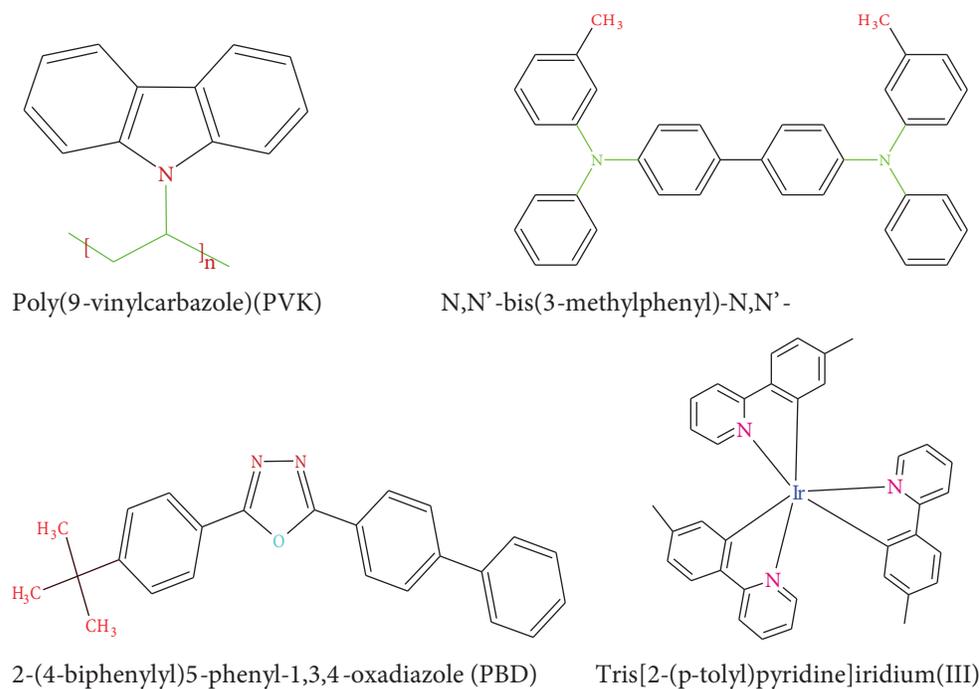
1. Introduction

The organic light-emitting diode (OLED) can play a key role in the new boundary of lighting, appearing to outdate Edison's invention that just over a century ago changed the life of mankind and also display technology. Some advantages of OLEDs that make them perfect candidates to replace the widely used liquid crystal displays and plasma display panels include high efficiency, low voltage, full color, and easy fabrication process as large area flat panel displays in electronic devices [1–3]. OLEDs have been recognized as a promising alternative display and lighting technology because of their unique advantages such as paper-like thickness, faster response, high contrast, power-saving abilities, and potential to be used for flexible applications [4–8]. The emission process of OLEDs involves the recombination of electrons and holes, which form 1 of 2 types of excited states: singlet and triplet. An important distinction of these 2 states is that the singlets can relax radiatively, whereas for the triplet states, this process is forbidden and, therefore, relaxation occurs via a nonradiative process. Simple spin statistics suggest that the ratio of singlets to triplets is 1:3, although studies show that this is not applicable in polymeric materials [9]. Phosphorescent OLEDs have been attracting much attention since the first report of Baldo et al. [10]. Today a huge number of phosphorescent dyes are used in phosphorescent OLEDs, utilizing different metal complexes containing transition metals such as iridium, platinum, osmium, or ruthenium. These transition metal complexes definitely exhibit a series of very desirable material properties such as emission wavelengths covering the entire visible spectrum, high quantum efficiency yields, and long

---

lifetimes. However, severe concentration quenching is observed for most pure layers of phosphorescent dyes. Consequently, phosphorescent dyes are usually blended into suitable host material (small molecules or polymers) from which the excitation energy is transferred to the phosphorescent guest.

OLEDs based on phosphorescent transition metal complexes are attracting significant attention since they can greatly improve electroluminescence (EL) performance as compared with the conventional fluorescent OLEDs [11–13]. According to spin statistics, the EL from small molecular fluorophores cannot exceed a maximum quantum yield of 25%, but in phosphorescent complexes, the EL can theoretically achieve quantum yields of up to 100% since both triplet and singlet excitons can be harvested for the emission [14]. Among all the phosphors, cyclometalated iridium(III) complexes are acquiring a mainstream position in the field of organic displays because of their highly efficient emission properties, relatively short excited state lifetime, and excellent color tunability over the entire visible spectrum [15,16].

Here we report the efficient and low-driving voltage behavior of green phosphorescent OLED devices with proper light emitting host profile. In this device configuration, we have used the Ir complex tris(2-(4-tolyl) phenylpyridine) iridium (Ir(mppy)$_3$) because of its relatively short excited state lifetime and high photoluminescence (PL) efficiency. We have fabricated OLEDs in an ITO/PEDOT:PSS/PVK:TPD:PBD:Ir(mppy)$_3$/LiF/Al device configuration. Thickness dependence study was carried out for phosphorescent OLED devices to see the direct relationship between thicknesses of active layers and device efficiencies. PVK:TPD:PBD:Ir(mppy)$_3$ active layer thicknesses were changed from 35 nm to 90 nm. The schematic OLED is presented in Figure 1.

Poly(9-vinylcarbazole)(PVK)

N,N'-bis(3-methylphenyl)-N,N'-

2-(4-biphenylyl)5-phenyl-1,3,4-oxadiazole (PBD)

Tris[2-(p-tolyl)pyridine]iridium(III)

Figure 1. The molecular structure of active layer materials.

2. Experimental section

All materials are of reagent grade and were used as received unless otherwise noted.

2.1. Materials

Poly(9-vinylcarbazole) (PVK), N,N'-bis(3-methylphenyl)-N,N'-diphenylbenzidine, 2-(4-biphenylyl)5-phenyl-1,3,4-oxadiazole (PBD), and tris[2-(p-tolyl)pyridine]iridium(III) were purchased from Aldrich. The molecular structures of the materials used as active layers are shown in Figure 2.

2.2. Device fabrication and characterization

Four OLED devices were manufactured with a variation of organic layer thickness. Active layer combinations were used with an indium tin oxide (ITO)/PEDOT:PSS (35 nm)/Ir(mppy)$_3$ (6 wt.%): PBD (24 wt.%): TPD (9 wt.%): PVK(61 wt.%)/LiF (0.7 nm)/Al (100 nm) device structure.

OLED devices were fabricated in the following configurations: ITO/PEDOT:PSS (35 nm)/PVK:TPD: PBD:Ir(mppy)$_3$ (35 nm)/LiF (0.7 nm)/Al (100 nm) (device SH1), ITO/PEDOT:PSS (35 nm)/PVK:TPD:PBD: Ir(mppy)$_3$ (40 nm)/LiF (0.7 nm)/Al (100 nm) (device SH4), ITO/PEDOT:PSS (35 nm)/PVK:TPD:PBD:Ir (mppy)$_3$ (56 nm)/LiF (0.7 nm)/Al (100 nm) (device SH3), and ITO/PEDOT:PSS (35 nm)/PVK:TPD:PBD:Ir (mppy)$_3$ (90 nm)/LiF (0.7 nm)/Al (100 nm) (device SH2). The ITO substrates were patterned by a conventional wet-etching process using an acidic mixture of HCl and H_2SO_4 as the etching agent. Patterned ITO glasses were cleaned with acetone, isopropanol, and ethanol by ultrasonic bath for 15 min, then dried and finally treated in a UV/O$_3$ cleaner. PEDOT:PSS (35 nm) was spin-coated at 4000 rpm on ITO glass. The PEDOT:PSS layers were baked at 120 °C for 5 min to remove residual water and then samples were annealed at 80 °C for 30 min. A blend of PVK:TPD:PBD:Ir(mppy)$_3$ in chlorobenzene solution was spin-coated on top of the ITO substrate precoated with PEDOT:PSS layer. An ultrathin LiF interfacial layer with a nominal thickness of 0.7 nm was incorporated between the polymer and the aluminum metal cathode to promote electron injection. The devices were prepared after the thermally evaporated cathode layer. The schematic energy diagram of the device and schematic OLED configuration are presented in Figures 2 and 3, respectively. All device fabrication and characterization processes were carried out under nitrogen atmosphere in a glove box system (MBRAUN, Germany) integrated with a device fabrication and characterization unit. Current and voltage characteristics were measured with an Agilent Technologies B1500A semiconductor device analyzer. The EL spectra and brightness of the devices were recorded with a Spectra Scan 655 spectroradiometer, Ocean Optics Q65000 fiberoptic spectrometer, and Admesy Brontes colorimeter. The film thicknesses were measured by Veeco Dektak 150 Profilometer. The Dektak is a profilometer for measuring step heights or trench depths on a surface. This is a surface contact measurement technique where a very low force stylus is dragged across a surface.
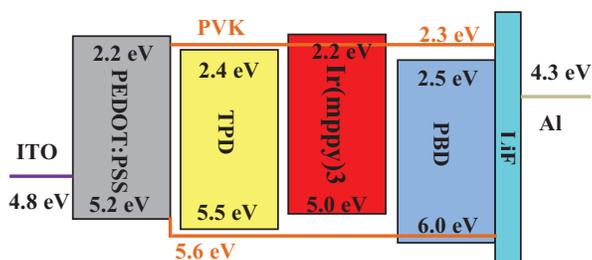

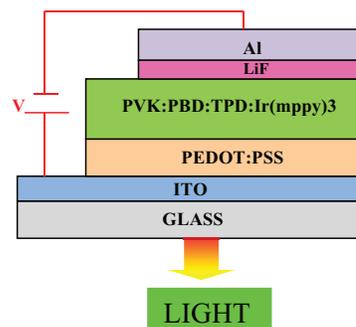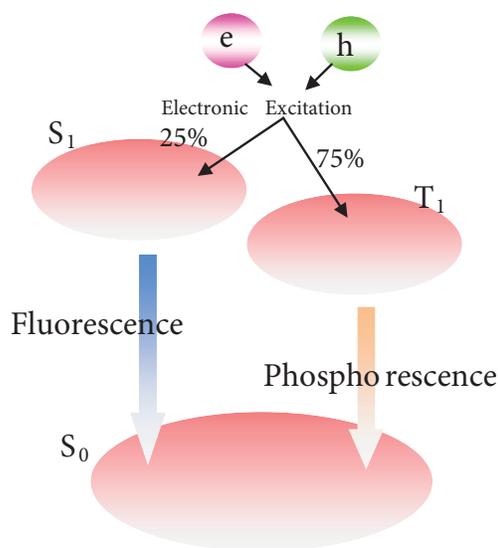**Figure 2.** The energy diagram of the device.

Figure 3. The structure of the device.

3. Results and discussion

Effects of the active layer of polymer light emitting diodes (PLED) on electrical and optical characteristics were systematically investigated. Phosphorescent PLEDs usually use a phosphorescent dye doped into a proper polymer matrix because they need the polymer matrix as host with a larger triplet state energy (T_1) than that of phosphorescent guest. In the case of $Ir(mppy)_3$ with a triplet energy of about 3 eV, mostly nonconjugated large band gap polymers such as PVK have been used in order to guarantee confinement of the triplet excited state on the guest and to optimize the balance of the charge–carrier injection and transport. Because of the poor electron transporting properties of PVK, electron transporting materials such as PBD are used to facilitate electron transport, causing good efficiencies and low driving voltages. In these PVK based phosphorescent PLEDs, the guest emission in the EL spectrum was far more intense than in the PL spectrum. This effect suggests that carrier trapping and subsequent recombination on the guest rather than energy transfer was the dominant excitation path of the triplet excited state of the phosphorescent guest. Additionally, for direct carrier trapping on the phosphorescent dye, a significant offset of the highest occupied molecular orbital (HOMO) and lowest unoccupied molecular orbital (LUMO) energies of the host and guest material was necessary, as schematically depicted in Figure 4.
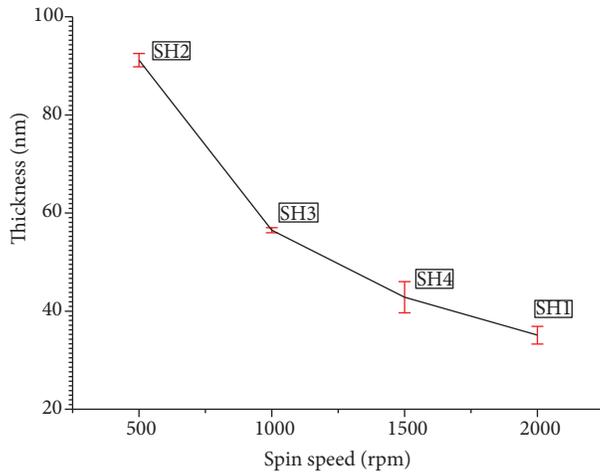

Figure 4. Triplet dynamics in a host–guest system.

Even though the direct formation of the guest triplet state was the most elegant way to achieve good color purity and high efficiency, it was often accompanied by a high operating voltage due to the build-up of a space-charge field.
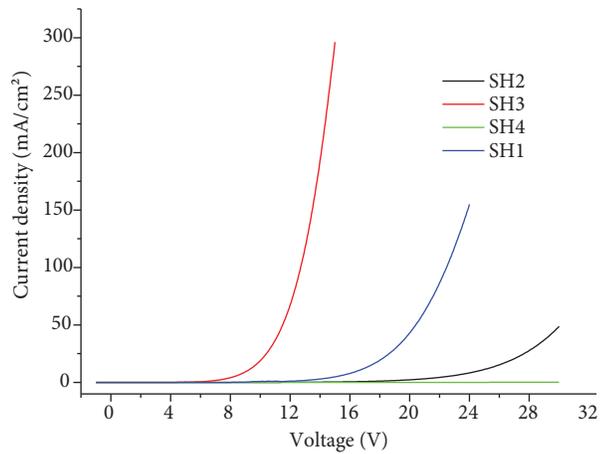
Comparing the HOMO energy of the chemically related $Ir(mppy)_3$ and PVK at –5.6 eV and –5 eV respectively, it was evident that the guest constituted a hole trap with depth of 0.6 eV. The direct hopping of holes between Ir dyes without the need for detrapping to PVK becomes possible by utilizing hole transporting molecules such as N-N'-diphenyl-N,N'-(bis(3-methylphenyl)-[1,1-biphenyl]-4,4'-diamine (TPD) doped in PVK. In addition, hole injection from the poly(3,4-ethylenedioxy thiophene):poly(styrene sulfonate) (PEDOT:PSS) anode might be facilitated via decreasing the charge injection barrier between HOMO levels of PEDOT:PSS and PVK.

The energy diagram of the device is presented in this study. Since polymers generally crosslink or decompose upon heating, they cannot be thermally evaporated in a vacuum chamber and hence they are generally deposited by spin-coating a thin film from a solution containing them. The thickness of spin-coated films may be controlled by the concentration of the polymer in the solution, the spinning rate, and the spin-coating temperature.
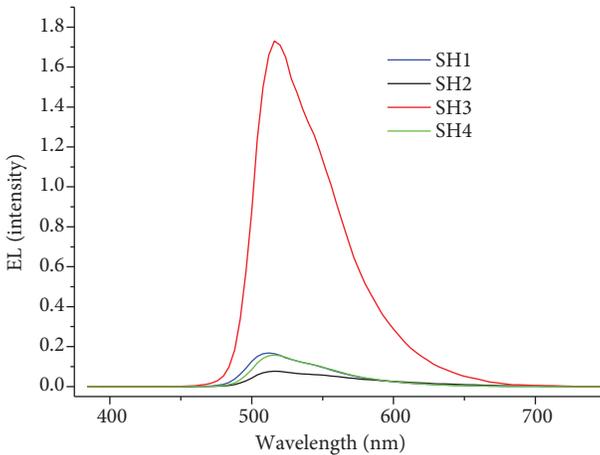
All electrical and optical properties are shown in Figures 5–8 and are summarized in the Table.
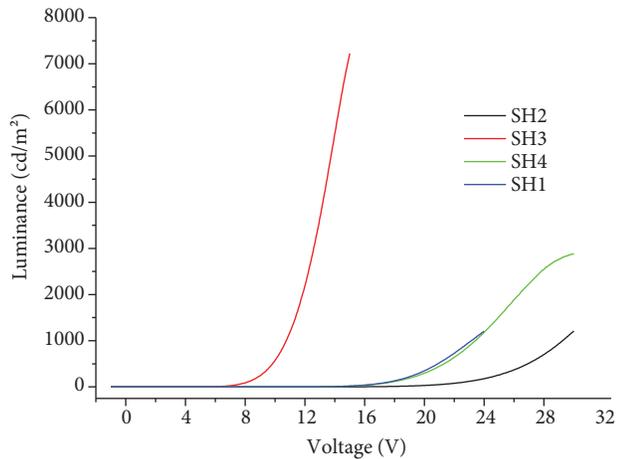
Figure 5. Spin speed–thickness curve.

Figure 6. Current density–voltage curve.
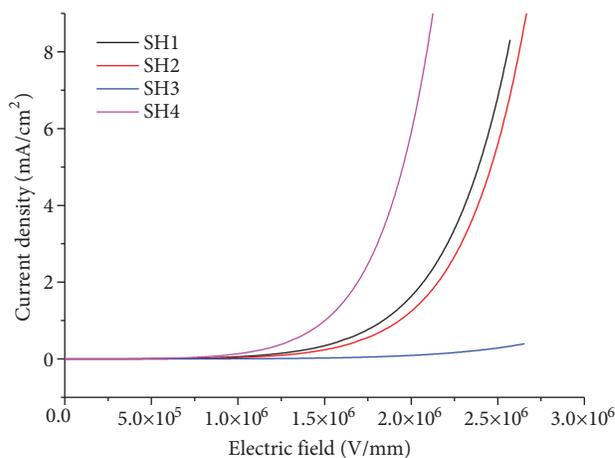
Figure 7. Wavelength–EL intensity curve.

Figure 8. Voltage–luminance curve.

Table. The performance of the devices.

Sample name	Turn-on voltage (V)	EL intensity (a.u.)	Max. luminance (Cd m^{-2})
SH1	3.3	1680	53.72
SH2	11.5	767	31.04
SH3	3.6	17300	575.5
SH4	3.7	1580	50.3

The relation between spin speed and active layer thickness is shown in Figure 5. Thickness decreases with increasing spin speed at room temperature in Figure 5. The current density-voltage (I-V) for devices with different active layer thicknesses, ranging from 35 nm to 95 nm, is shown in Figure 6. As was expected, threshold voltage increased with active layer thickness, not only due to the limiting effect of the bulk current, but also due to a decrease of the injection rate, associated with a reduction of the internal electric field at the interface. The best device in terms of lowest threshold voltage is the device with active layer of 56 nm. The EL spectra of the devices are shown in Figure 7, in which the peak of the EL spectrum of the SH3 device was centered at 512 nm. The V-L characteristics of 4 devices with different active layer thicknesses are presented in Figure 8, where we can see that device SH3 (56 nm thickness) has the highest luminance of 575.5 cd m^{-2} at 2.8 mA.

The current density-electric field characteristics of PLED devices are presented in Figure 9. In these devices, I-V characteristics not only depend on voltage but also strongly depend on electric field. Insulator/metal devices work for electric field induced tunneling. This clearly points to a tunneling model for carrier injection in which one or both carriers is field emitted through a barrier at the electrode/polymer interface [17]. Electrons and holes, injected from contacts into the polymer, form negatively and positively charged polarons in the polymer. These polarons migrate under the influence of the applied electric field, forming a polaron exciton with an oppositely charged field, forming a polaron exciton with an oppositely charged species and subsequently undergoing radiative recombination [17].

Figure 9. Current density–electric field characteristic curve.

4. Conclusion

OLEDs in a ITO/PEDOT:PSS/PVK:TPD:PBD:Ir(mppy)$_3$/LiF/Al device configuration were successfully fabricated. The study of thickness dependence was carried out for OLED devices. Active layers were spin-coated with different spin speeds of 2000 rpm, 1500 rpm, 1000 rpm, and 500 rpm. Spin speed changed the active layer thicknesses at 35 nm, 40 nm, 56 nm, and 90 nm, respectively. The optimum thickness was determined as 56 nm for the PVK:TPD:PBD:Ir(mppy)$_3$ active layer. The characteristics of the devices were studied using the device with active layer thickness of 56 nm, which produced lower turn-on voltage of 3.6 V and gave the highest luminance of 575.5 cd m^{-2}. As a result, experiments showed that OLED device efficiencies were dependent on active layer thicknesses.

Acknowledgments

References

[1] Tang, C. W.; VanSlyke, S. A. *Appl. Phys. Lett.* **1987**, *12*, 913–915.

[2] Lamansky, S.; Djurovich, P.; Murphy, D.; Abdel-Razzaq, F.; Lee, H. E.; Adachi, C.; Burrows, P. E.; Forrest, S.R.; Thompson, M. E. *Chem. Soc.* **2001**, *18*, 4304–4312.

[3] Sun, Y.; Giebink, N. C.; Kanno, H.; Ma, B.; Thompson, M. E.; Forrest, S. R. *Nature* **2006**, *440*, 908–912.

[4] Reineke, S.; Lindner, F.; Schwartz, G.; Seidler, N.; Walzer, K.; Lüssem, B.; Leo, K. *Nature* **2009**, *459*, 234–238.

[5] Adachi, C.; Baldo, M. A.; Forrest, S. R.; Thompson, M. E. *Appl. Phys. Lett.* **2000**, *77*, 904–907.

[6] Baldo, M. A.; Lamansky, S.; Burrows, P. E.; Thompson, M. E.; Forrest, S. R. *Appl. Phys. Lett.* **1999**, *75*, 4–6.

[7] Duan, L.; Hou, L.; Lee, T. W.; Qiao, J.; Zhang, D.; Dong, G.; Wang, L.; Qiu, Y. *J. Mater. Chem.* **2010**, *20*, 6392–6407.

[8] Forrest, S. R. *Nature* **2004**, *428*, 911–918.

[9] Walker, B.; Tamayo, A.; Yang, J.; Brzezinski, J. Z.; Nguyen, T. Q. *Appl. Phys. Lett.* **2008**, *93*, 063302–063305.

[10] Baldo, M. A.; O'Brien, D. F.; You, Y.; Shoustikov, A.; Sibley, S.; Thomson, M. E.; Forrest, S. R. *Nature* **1998**, *395*, 151–154.

[11] Fisher, A. L.; Linton, K. E.; Kamtekar, K. T.; Pearson, C.; Bryce, M. R.; Petty, M. C. *Chem. Mater.* **2011**, *23*, 1640–1642.

[12] Lee, T. W.; Noh, T.; Shin, H. W.; Kwon, O.; Park, J. J.; Choi, B. K.; Kim, M. S.; Shin, D. W.; Kim, Y. R. *Adv. Funct. Mater.* **2009**, *19*, 1625–1630.

[13] Xiao, L.; Chen, Z.; Qu, B.; Luo, J.; Kong, S.; Gong, Q.; Kido, J. *Adv. Mater.* **2011**, *23*, 926–952.

[14] Khalifa, M. B.; Mazzeo, M.; Maiorano, V.; Mariano, F.; Carallo, S.; Melcarne, A.; Cingolani, R.; Gigli, G. *J. Phys. D.* **2008**, *41*, 155111.

[15] Kawamura, Y.; Goushi, K.; Brooks, J.; Brown, J. J.; Sasabe, H.; Adachi, C. *Appl. Phys. Lett.* **2005**, *86*, 071104.

[16] Baldo, M. A.; Thompson, M.E.; Forrest, S. R. *Nature* **2000**, *403*, 750–753.

[17] Parker, I. D. *J. Appl. Phys.* **2000**, *75*, 1656–1666.